Climate Simulation and Future Projection of Precipitation and the Water Vapor Budget in the Haihe River Basin

LI Qiaoping* (李巧萍) and DING Yihui (丁一汇)

National Climate Center, China Meteorological Administration, Beijing 100081

(Received July 12, 2011; in final form December 28, 2011)

ABSTRACT

The climatological characteristics of precipitation and the water vapor budget in the Haihe River basin (HRB) are analyzed using daily observations at 740 stations in China in 1951–2007 and the 4-time daily ERA40 reanalysis data in 1958–2001. The results show that precipitation and surface air temperature present significant interannual and interdecadal variability, with cold and wet conditions before the 1970s but warm and dry conditions after the 1980s. Precipitation has reduced substantially since the 1990s, with a continued increase of surface air temperature. The total column water vapor has also reduced remarkably since the late 1970s. The multi-model ensemble from the Fourth Assessment Report (AR4) of the Intergovernmental Panel on Climate Change (IPCC) has capably simulated the 20th century climate features and successfully reproduced the spatial patterns of precipitation and temperature. Unfortunately, the models do not reproduce the interdecadal changes. Based on these results, future projections of the climate in the HRB are discussed under the IPCC Special Report on Emissions Scenarios (SRES) B1, A1B, and A2. The results show that precipitation is expected to increase in the 21st century, with substantial interannual fluctuations relative to the models' baseline climatology. A weak increasing trend in precipitation is projected before the 2040s, followed by an abrupt increase after the 2040s, especially in winter. Precipitation is projected to increase by 10%–18% by the end of the 21st century. Due to the persistent warming of surface air temperature, water vapor content in the lower troposphere is projected to increase. Relative humidity will decrease in the mid-lower troposphere but increase in the upper troposphere. On the other hand, precipitation minus evaporation remains positive throughout the 21st century. Based on these projection results, the HRB region is expected to get wetter in the 21st century due to global warming.

Key words: the Haihe River basin, precipitation, water vapor budget, simulation and projection

Citation: Li Qiaoping and Ding Yihui, 2012: Climate simulation and future projection of precipitation and the water vapor budget in the Haihe River basin. *Acta Meteor. Sinica*, **26**(3), 345–361, doi: 10.1007/s13351-012-0307-9.

1. Introduction

In the last 100 years, temperatures have tended to warm significantly both globally and in China, accompanied by rising sea levels and rapid thawing of glaciers and icecaps. Extreme climate events such as high temperatures, droughts, heavy precipitation, and strong storms tend to be more frequent and stronger (IPCC, 2007). Under the background of global warming, the increasingly prominent problems of water resources not only threaten water supply safety and food security, but also lead to a series of ecological and environmental issues. More and more attention has been focused on the impacts of climate change on water resources in drainage basins in China (Liu et al., 2008; Wang et al., 2008; Zhang Liping et al., 2008; Jiang Tong et al., 2005; Guo et al., 2007; Zeng et al., 2007). The Haihe River basin (HRB) includes three large water systems (Luanhe, Haihe, and Tuhaimajiahe rivers), and belongs to a semi-drought or semi-wet continental monsoon climate in the temperate zone. Precipitation in the HRB is concentrated mainly in summer; therefore, summer precipitation directly determines water resources and the drought-wet status. The shortage of water resources in the HRB has become a growing problem in recent years, influenced by global climate

Supported by the National Science and Technology Support Program of China (2007BAC03A01), China Meteorological Administration Special Public Welfare Research Fund (GYHY200906020 and GYHY200806006), and National Basic Research and Development (973) Program of China (2006CB403404).

*Corresponding author: liqp@cma.gov.cn.

change, intensive human activities, and environment deterioration, and representing a key restriction on social and economic development (Ye and Huang, 1996; Shi et al., 1995). Annual runoff of HRB has decreased sharply by about 66%, from 3.24×10^{11} m^3 in the 1950s to 1.11×10^{11} m^3 at present (Water Resources Committee for the Haihe River Basin, 2006). In the past 20 years, groundwater levels in the HRB have fallen by approximately 1 m in shallow areas and by more than 2 m in deep areas (Wang and Huang, 2004). Furthermore, in the past 50 years, the total water consumption has increased by a factor of about 4.4, with the average amount per person rising by a factor of about 1.5 (Wang et al., 2008). The shortage of water resource is becoming more and more serious due to increasing water requirements. Meanwhile, pollution of surface water and groundwater in the HRB is also becoming more severe, further exacerbating the shortage of water resources. Under the background of global warming, future climate change would directly affect the environmental and agricultural development in the HRB.

In this paper, the climatological characteristics of precipitation and the water vapor budget in the HRB since 1951 are analyzed. The ability of climate models in simulating interannual and interdecadal variability of rainfall is evaluated using the multi-model ensemble from the Fourth Assessment Report of the Intergovernmental Panel on Climate Change (IPCC AR4; IPCC, 2007). Future climate change trends are analyzed based on the ensemble results under the Special Report on Emissions Scenarios (SRES) B1, A1B, and A2.

Most of the previous studies focus on the climatological characteristics and future changes of precipitation and surface air temperature. In this paper, interannual and interdecadal variations of precipitation and the water vapor budget in the past 50 years and the model capability are analyzed. Furthermore, future projections of the water vapor budget in the HRB are conducted and discussed. This study aims to provide a scientific basis for research on the eco-environment rehabilitation and agricultural production in the HRB.

The paper is organized as follows. Section 2 introduces the data and methods. The climatological characteristics of precipitation and the water vapor budget in the HRB based on observational data since 1951 are discussed in Section 3. Model performance in simulating the recent climatology is discussed in Section 4. Future projections of precipitation and the water vapor budget in the study regions are presented in Section 5. The results are discussed and summarized in Section 6.

2. Data and methods

2.1 Data

Datasets used in this paper include:

(1) Daily observations of precipitation and surface air temperature at 740 stations in China from 1951 to 2007.

(2) European Centre for Medium-Range Weather Forecasts (ECMWF) 40-yr 4-time daily reanalysis data (ERA40) on a $2.5°\times2.5°$ resolution from 1958 to 2001 (http://www.ecmwf.int/research/era/Project/Plan/Project_plan_TOC.html).

(3) Monthly mean data from the multi-model ensemble and some individual models from the IPCC AR4 model simulations for 1951–2000 (20C3M experiments) and 2001–2099 (SRES B1, A1B, and A2 experiments). The ensemble data are collected and analyzed by the National Climate Center of China (http://ncc.cma.gov.cn) and the output from individual models has been downloaded from http://www-pcmdi.llnl.gov/ipcc/about_ipcc.php. The models that participated in the IPCC AR4 represent an advanced state of climate modeling and have improvements relative to those that participated in the IPCC Third Assessment Report (TAR), with relatively higher precision, more reasonable parameterization schemes, and updated numerical methods. More information on the models can be found at the above website.

2.2 Methods

In this paper, the multi-model ensemble for the 20C3M experiments is just a simple arithmetic average with equal weights for all individual models. Jiang

Dabang et al. (2005) reported that the multi-model ensemble mean is always more reliable than any single model in simulating the climatology of annual and seasonal precipitation in East Asia. The numbers of models are different for different emission scenarios, with 17 models for SRES A1B, 16 models for SRES A2, and 17 models for SRES B1. All of the results are interpolated onto equidistant grids (1.0°×1.0°). The details are available at http://ncc.cma.gov.cn.

The root mean square error (RMSE) is calculated to provide an overview of the models' capability in simulating precipitation and the water vapor budget in the HRB (35°–43°N, 112°–120°E):

$$\mathrm{RMSE}=\sqrt{\frac{1}{n}\sum_{i=1}^{n}(x_{i\mathrm{m}}-x_{i\mathrm{obs}})^2}. \tag{1}$$

In Eq. (1), $x_{i\mathrm{m}}$ ($x_{i\mathrm{obs}}$) denotes the model simulated (observed) value at the ith spatial grid point of the domain; n is the total number of grid points within the domain; RMSE is root mean square error between the simulation and the observation.

The Mann-Kendall test (Mann, 1945; Kendall, 1975) and the Morlet wavelet transform method (Grossmann and Morlet, 1984) are used to investigate decadal variations in the observed and simulated time series of rainfall (Wei, 2007).

In order to understand the climatological characteristics and future trends of water vapor transport, zonal and meridional water vapor transports are calculated as follows:

$$Q_u=\frac{1}{g}\int_{p_\mathrm{s}}^{300} q(\lambda,\phi,p,t)u(\lambda,\phi,p,t)\mathrm{d}p, \tag{2}$$

$$Q_v=\frac{1}{g}\int_{p_\mathrm{s}}^{300} q(\lambda,\phi,p,t)v(\lambda,\phi,p,t)\mathrm{d}p, \tag{3}$$

where Q_u and Q_v are the zonal and meridional moisture fluxes; q is specific humidity; u and v are the zonal and meridional wind components, respectively; g is the gravitational constant; p_s is surface pressure; λ, ϕ, t, and p are longitude, latitude, time, and pressure, respectively; and 300 hPa is the uppermost air pressure in the integral. The water vapor fluxes at the four borders (west, east, south, and north) of the HRB are defined as:

$$Q_\mathrm{W}=\sum_{y=\phi_1}^{\phi_2} Q_u(\lambda_1,y,t), \tag{4}$$

$$Q_\mathrm{E}=\sum_{y=\phi_1}^{\phi_2} Q_u(\lambda_2,y,t), \tag{5}$$

$$Q_\mathrm{S}=\sum_{x=\lambda_1}^{\lambda_2} Q_v(\phi_1,x,t), \tag{6}$$

$$Q_\mathrm{N}=\sum_{x=\lambda_1}^{\lambda_2} Q_v(\phi_2,x,t), \tag{7}$$

$$Q_\mathrm{T}=Q_\mathrm{W}-Q_\mathrm{E}+Q_\mathrm{S}-Q_\mathrm{N}. \tag{8}$$

$Q_\mathrm{W}, Q_\mathrm{E}, Q_\mathrm{S}$, and Q_N denote water vapor flux from the western, eastern, southern, and northern borders of the domain, respectively. Q_T is the total or net water vapor budget. $\lambda_1, \lambda_2, \phi_1$, and ϕ_2 represent the longitude and latitude of the borders.

Relative humidity is also calculated for discussion of possible future changes of atmospheric humidity:

$$e_\mathrm{s}(T)=6.11\exp\left[\frac{\mathrm{a}(T-273.16)}{T-\mathrm{b}}\right], \tag{9}$$

$$q_\mathrm{s}=\frac{0.622e_\mathrm{s}(T)}{p-0.378e_\mathrm{s}(T)}, \tag{10}$$

$$\mathrm{RH}=\frac{q}{q_\mathrm{s}}\times 100, \tag{11}$$

where $e_\mathrm{s}(T)$ is saturation vapor pressure and T denotes temperature. The values of the constants a and b are 17.26 and 35.86 for temperatures above 0℃ and 21.87 and 7.66 for temperatures below 0℃. The variable q_s denotes saturation specific humidity, p is pressure, q is specific humidity, and RH is relative humidity (Ding, 1989).

3. Observed climatology

Analysis of the station observations in China indicates that the distribution of annual precipitation in HRB is latitudinal, with an apparent increase in precipitation from north to south (figure omitted). Rainfall totals only 300 mm in the northern part, along the common boundary of Shanxi and Inner Mongolia, but about 700 mm in the southern part, near the Yellow River basin. The northern and southern parts are separated by a distinguishing line along the Taihang Mountains. Rainfall occurs mainly during summer with the southwesterly monsoon, which accounts for more than 50% of the annual total. Little precipitation (only 10–30 mm) occurs during winter, especially in the northern region. Regional differences are also apparent in the distribution of mean surface air temperature (figure omitted). The regions between eastern Inner Mongolia and northern Shanxi Province are cooler than the southeastern and coastal regions. Wutai Mountain is the coldest region because its elevation is the highest.

Figure 1 shows annual normalized precipitation and temperature anomalies during 1951–2007, with 1961–1990 as the base period. Annual precipitation in the HRB decreased over this time period at a rate of –18.3 mm (10 yr)$^{-1}$. Approximately, the evolution of rainfall has occurred in three different stages since 1951 (Fig. 1a). It was wet before 1965, then transformed from wet to dry with obvious interannual fluctuations during the mid 1960s to mid 1970s. Drought has occurred frequently since the late 1970s, and total precipitation has decreased significantly especially in the most recent decade. Rainfall in 2002 was 28% below the 1961–1990 mean. The evolution of summer rainfall is consistent with that of annual rainfall. Rainfall was abundant during the mid 1950s to 1960s. For example, rainfall exceeded the baseline value by more than 30% in 1956, 1958, and 1964. However, drought occurred persistently from the 1980s to the early 1990s, with particularly severe droughts in the mid 1990s. The summer rainfall in 1997 was approximately 40% below the baseline value, representing the most severe drought year in the past 50 years. Severe drought events also occurred in 1999, 2002, and 2005. Drought is a dominant climatological feature in the HRB over the most recent 30 years.

Annual mean surface air temperature in the HRB rose significantly over the period 1951–2007, with a warming trend of 0.32℃ (10 yr)$^{-1}$ (Fig. 1b). The years before the early 1970s were substantially cooler than the baseline period, especially the years of 1952–1957. Thereafter, annual mean temperature typically fluctuated within a small range through the mid 1970s and 1980s. The temperature has risen steadily since 1987, with annual mean temperature more than 1℃

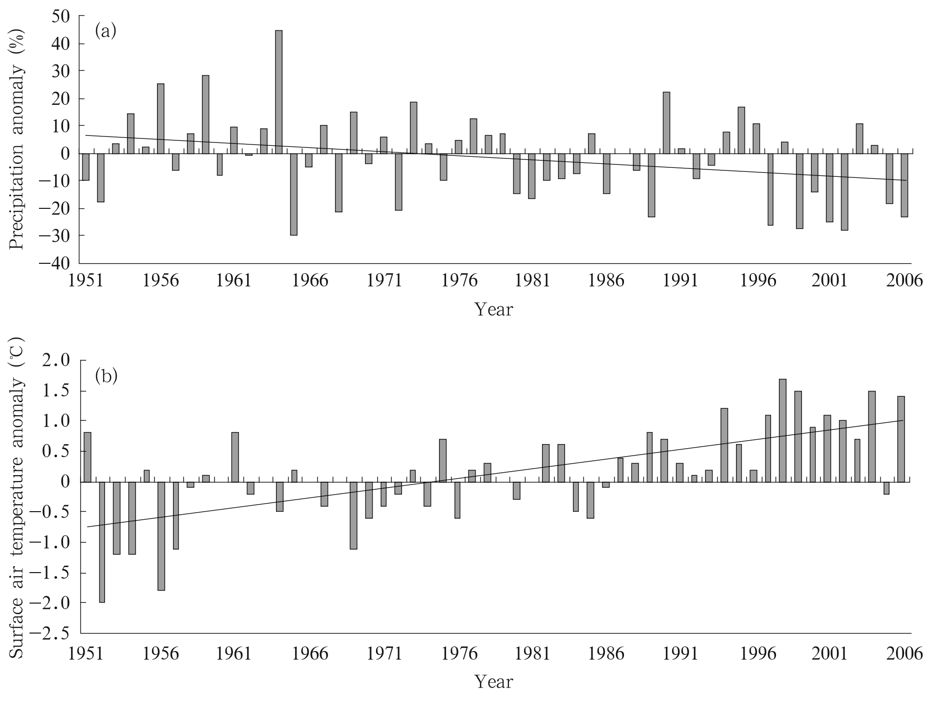

Fig. 1. Time series of annual anomalies of (a) precipitation (%) and (b) surface air temperature (℃). The solid lines indicate the linear trends.

warmer than the baseline in most years of the period 1987–2007.

Table 1 shows decadal variations in annual mean and summer mean precipitation and surface air temperature relative to baseline averages from 1961 to 1990. The climatological patterns for the periods of 1951–1970 and 1981–2007 are apparently different. Conditions were relatively cool and wet before the 1970s, then relatively warm and dry since the 1980s. Precipitation decreased and temperature increased more significantly after the 1990s. Annual mean temperature increased by 0.9℃ during the period of 2001–2007, indicative of serious drought in the HRB over the most recent decade.

Water vapor fluxes through each border are calculated, along with a regional water vapor budget for the HRB. The water vapor budget is calculated along the boundaries of 35°N, 42.5°N, 112.5°E, and 120°E, respectively. The results indicate that the input of water vapor at the western boundary is less than the output of water vapor from the eastern boundary, leading to a negative net zonal water vapor transport. The net meridional transport is positive because the input from the southern boundary exceeds the output from the northern boundary. The net water vapor budget in the area was large before the 1960s, but decreased substantially from the 1980s, and its value in the 1990s was only 20% of that in the 1960s. The net water vapor budget over the HRB has also reduced since the late 1970s, especially in summer. This reduction is consistent with the interdecadal variations of precipitation in the area (Table 2). The decrease of net water vapor budget mainly results from a significant reduction in the meridional transport, which suggests a decrease in the amount of water vapor entering the region from the southern boundary.

4. Multi-model simulation

Some recent evaluations of the IPCC AR4 model simulations of precipitation in China and in the East Asian monsoon region indicate that most models can reproduce interannual variations and spatial patterns of precipitation in China. These models appear better in simulating precipitation in eastern China than in central and western China. Furthermore, most models can capture the seasonal jump and retreat of the major rain belt over eastern China (Zhang Li et al., 2008; Sun and Ding, 2008). However, individual models exhibit obvious differences in their simulation of the spatial distribution of the East Asian monsoon rainfall. Generally, the results from the multi-model ensemble are better than those from individual models (Sun and Ding, 2008). Most individual models perform better at simulating surface air temperature than precipitation; they reproduce the spatial features of temperature in China relatively well. Jiang et al. (2009) calculated the spatial correlation between the simulated surface air temperature from 17 IPCC AR4 models and the observations provided by the Climatic

Table 1. Decadal variations of precipitation anomaly (mm) and surface air temperature anomaly (℃)

	Precipitation		Surface air temperature	
	Annual	Summer	Annual	Summer
1950s	0.02	0.18	–0.63	–0.04
1960s	0.04	0.13	–0.18	0.14
1970s	0.04	0.10	–0.05	–0.13
1980s	–0.09	–0.30	0.22	0.06
1990s	–0.12	–0.27	0.78	0.60
2001–2007	–0.23	–0.73	0.92	0.63

Table 2. Summer water vapor budget(10^6 kg s^{-1}) along each boundary of the HRB

	West border	East border	South border	North border	Net budget
1960s	66.92	107.05	45.71	–2.51	8.09
1970s	67.78	101.07	35.19	0.61	1.29
1980s	81.14	101.55	32.35	8.63	3.31
1990s	53.76	85.79	27.66	–5.88	1.51

Research Unit (CRU). Their results indicate that the models perform well, with correlations of 0.948–0.992; unfortunately, a systematic cold bias exists in the simulated surface air temperatures in China (Jiang Dabang et al., 2005; Xu et al., 2007; Zhou and Yu, 2006).

Figure 2 shows the climatological spatial distributions of annual mean precipitation and surface air temperature from the multi-model ensemble simulation and the observation in the HRB, along with the RMSE. The simulated annual mean precipitation is very similar to the observation in the south of the Yellow River, but the magnitude is larger than that of the observation in the northern region. The spatial correlation between the simulated and the observed annual mean precipitation is 0.7057. The RMSE between the simulated and observed annual mean precipitation (Fig. 2c) suggests that the largest errors are concentrated in the coastal regions, with RMSE as high as 1.6–2.0 mm. For summer mean precipitation, the simulated spatial distribution in the Hetao

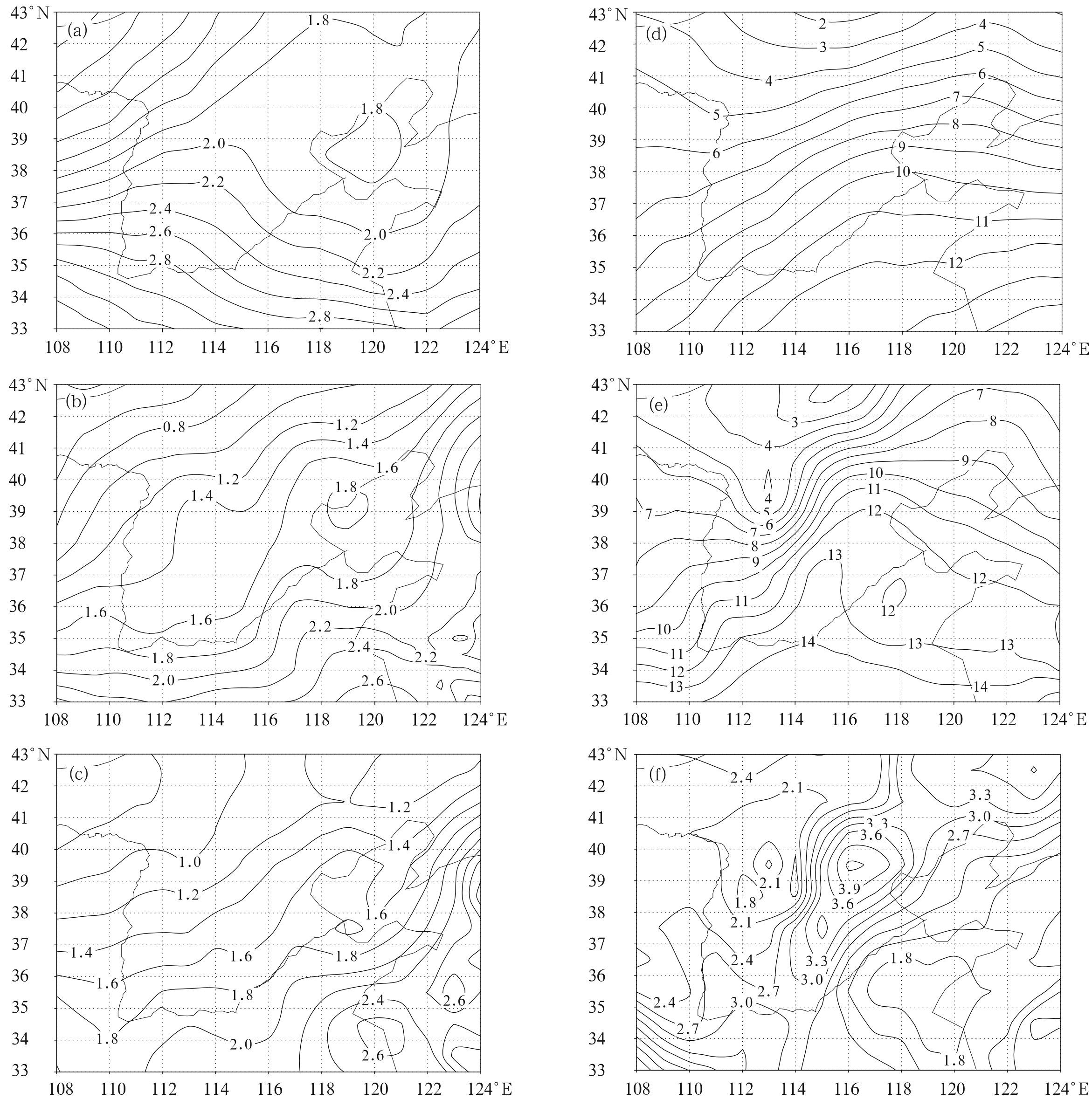

Fig. 2. Spatial distributions of annual mean precipitation (left panels; mm day^{-1}) and surface air temperature (right panels; ℃) from (a, d) simulation, (b, e) observation, and (c, f) their RMSE.

area and the eastern regions is consistent with that of the observation (figure omitted), but the amount of precipitation simulated in the regions of Tianjin and Tanggu is too small. The simulation exaggerates winter mean precipitation relative to the observation, especially along the coast of the Yellow River and the southern regions.

The simulated annual mean surface air temperature bears accurately the observed spatial features. The correlation between the simulated and observed annual mean surface air temperature is 0.9393, indicating that the ensemble mean depicts the spatial distribution of annual mean surface air temperature quite well. The observation (Fig. 2e) indicates the presence of a temperature trough in the eastern region and a temperature ridge in the western region. The simulated trough and ridge are weaker than those observed, mainly due to a warm bias in simulated annual mean temperature in Shanxi Province and a cold bias along the eastern coastline. The maximum RMSE is 3.9℃, located near Tianjin. The seasonal distribution of surface air temperature (figure omitted) indicates that the simulation accurately reproduces the spatial pattern of summer mean temperature, with exception of the cooling in northern Shanxi Province. The models perform better in winter than in summer.

We calculate the monthly errors in regional mean precipitation and surface air temperature between the simulations and observation. The results show that the precipitation bias is the smallest in autumn (–0.29 mm day^{-1}) and largest in spring (1.4 mm day^{-1}). The simulated precipitation exceeds the observed precipitation for most months, except for July, August, and September. The simulation exhibits a systematic cold bias relative to the observed surface air temperature, which ranges from –0.29℃ (in February) to –2.78℃ (in October). The annual mean bias is approximately –1.39℃. Monthly standard error between the simulated and observed surface air temperature (figure omitted) also indicates that the models have a consistent bias. Liu and Jiang (2009) reported that the mean error of simulated surface air temperature in China from the IPCC AR4 models relative to observations is approximately –6.694℃. This suggests that the simulations are better in the HRB than in China.

A model's performance should be evaluated based on not only the model's ability to reproduce the climatological spatial distribution, but also its ability to simulate interannual and interdecadal variability. Comparison between the simulated and observed percentage of annual precipitation anomalies in the recent 50 years (1951–2000) indicates that the ensemble mean reproduces the signs of departure for most years, with a significant correlation of 0.2960 between the ensemble mean and the observation. Unfortunately, the ensemble mean does not reproduce the linear decreasing trend in precipitation.

Application of the Mann-Kendall test to the precipitation time series indicates that the observed precipitation in the HRB experienced two significant abrupt change points, which occurred in 1982 and 1997, respectively. Application of the same test to the ensemble mean results identifies only one point in 1998 (figure omitted). Actually, the observed precipitation in the HRB experienced a significant interdecadal change in the 1980s (Fig. 1a). Molet wavelet transform analysis has also been applied to both the simulated and observed precipitation (Fig. 3). The results show that the simulated precipitation experiences obvious periodic cycles from dry and wet with a dominant interdecadal period of 12 years and a dominant interannual period associated with a quasi-biennial oscillation (Fig. 3a). These periods are different from those identified in the observational time series, which undergoes oscillations at periods of 16, 8, and 4 yr, respectively (Fig. 3b). This disagreement indicates that the ensemble mean of the IPCC AR4 models is relatively incapable of simulating interannual and interdecadal changes of precipitation in the HRB.

Sun and Ding (2008) classified 19 IPCC AR4 models into three categories based on each model's performance in simulating the interdecadal variations of summer precipitation and monsoon circulation in East Asia. Their study indicates that Category-1 and Category-2 models (9 models in total) can well reproduce interannual and interdecadal variations of precipitation in East Asia. We have also applied the Molet wavelet transform to precipitation in the HRB from

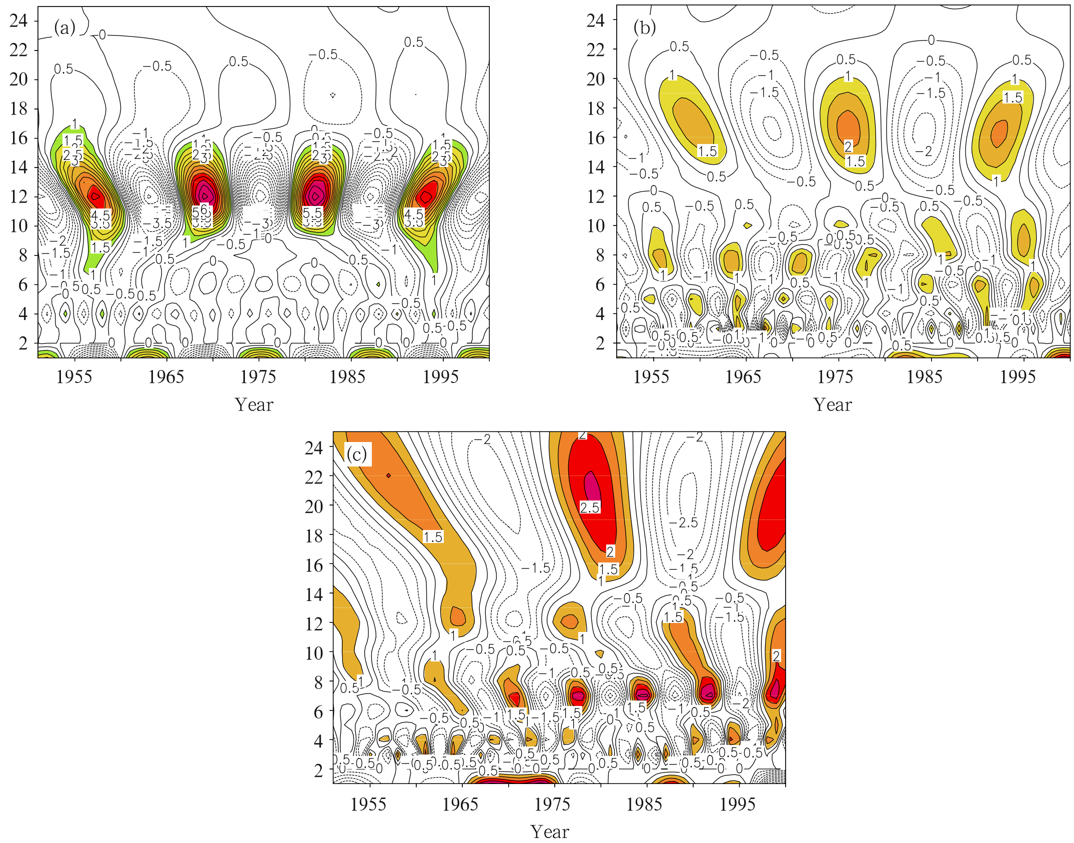

Fig. 3. Molet wavelet transform applied to annual precipitation in HRB from (a) the ensemble mean of all IPCC AR4 models, (b) observations, and (c) the ensemble mean of five selected models.

the 9 Category-1 and Category-2 models, i.e., the GFDL_CM2.0, MIROC3.2 (hires), MIROC3.2 (medres), CNRM_CM3, CSIRO, GFDL_CM2.1, INMCM2.0, UKMO_HadCM3, and GFEL_CM2.1 (Sun and Ding, 2008). The results suggest that the periodic cycles in the ensemble mean of these nine models are closer to those in the observational time series; however, the difference between simulated and real conditions is still obvious (figure omitted). Based on the capabilities of individual models in simulating anomalies in precipitation in the HRB during 1951–2000 (mainly the linear trend and correlation coefficients with the observations), we select five models (UKMO_HadGem1, MPI_Echam5, MIROC3.2(hires), GFEL_CM2.1, and CSIRO). Figure 3c shows the results of the Molet wavelet transform for the ensemble mean of these five models. This ensemble better simulates the interannual and interdecadal periodic cycles of precipitation in the HRB than does the ensemble that includes all models.

5. Possible 21st century changes in precipitation and the water vapor budget in HRB

5.1 Changes in precipitation

Figure 4 shows annual precipitation anomaly percentage in China and HRB in the 21st century, normalized by the mean climatology from 1980–1999. This provides a straightforward comparison with those reported in the IPCC AR4 (IPCC, 2007) and those by some previous studies in China (e.g., Sun and Ding, 2008). In addition, a 9-yr running average has been applied to remove annual variations in the time series of precipitation and surface air temperature. Precipitation in the HRB under the three SRES scenarios increases throughout the 21st century, especially after 2050. The mean precipitation trends under SRES scenarios B1, A1B, and A2 are 6.6, 13.5, and 13.5 mm

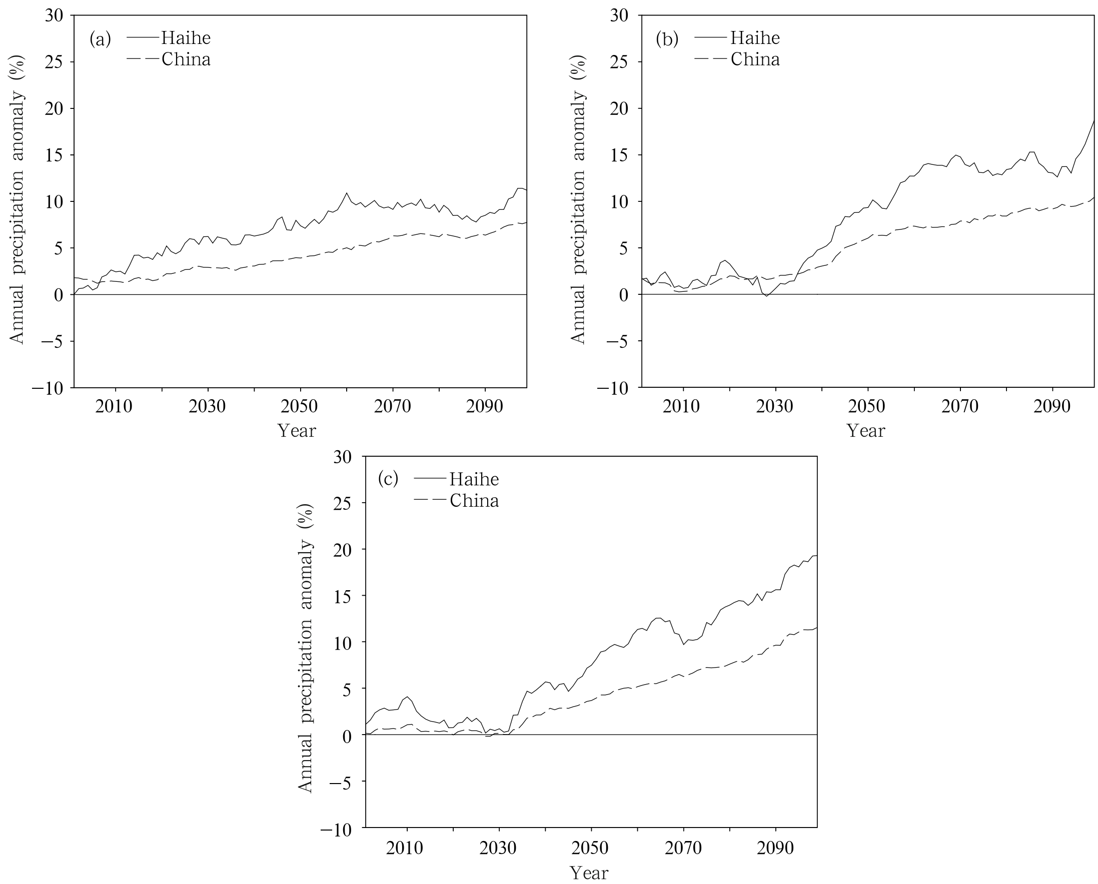

Fig. 4. Normalized annual precipitation anomalies (%) in the 21st century under SRES scenarios (a) B1, (b) A1B, and (c) A2.

$(10\ \mathrm{yr})^{-1}$, respectively. The magnitude of the increase under SRES B1 is smaller than that under SRES A1B or A2, with a relative increase of only about 7%. Precipitation is projected to increase significantly under the other two scenarios, with a maximum relative increase of 20%. By the end of the 21st century, the annual HRB precipitation amounts under SRES scenarios B1, A1B, and A2 are expected to increase by 10.2%, 14.7%, and 18%, respectively. These increases are higher than the nationwide average.

Mann-Kendall tests have been applied to the annual time series of precipitation in the HRB in the 21st century under the three SRES scenarios. The results show that abrupt change points in the precipitation time series are expected to occur in 2028 under scenario B1, in 2046 under A1B, and in 2059 under A2. The results of a previous study (Sun and Ding, 2008) suggest that precipitation in eastern China will increase in distinct stages in the 21st century, with relatively weak increases before the 2040s. Increases in precipitation are expected to become much more pronounced after the end of the 2040s, at which point the whole eastern China enters a wet period. The projected changes in precipitation in the HRB are therefore consistent with the projected changes in China. The ensemble mean from the aforementioned five models that more closely mirror observed changes during the latter part of the 20th century is similar to the ensemble mean of all models (figure omitted).

Figure 5 shows normalized seasonal precipitation anomalies in the HRB over the 21st century relative to the 1980–1999 baseline under the three SRES emission scenarios (B1, A1B, and A2). Precipitation is projected to increase most significantly in winter and spring, with smaller increases in summer and autumn. The projections under the three SRES scenarios do

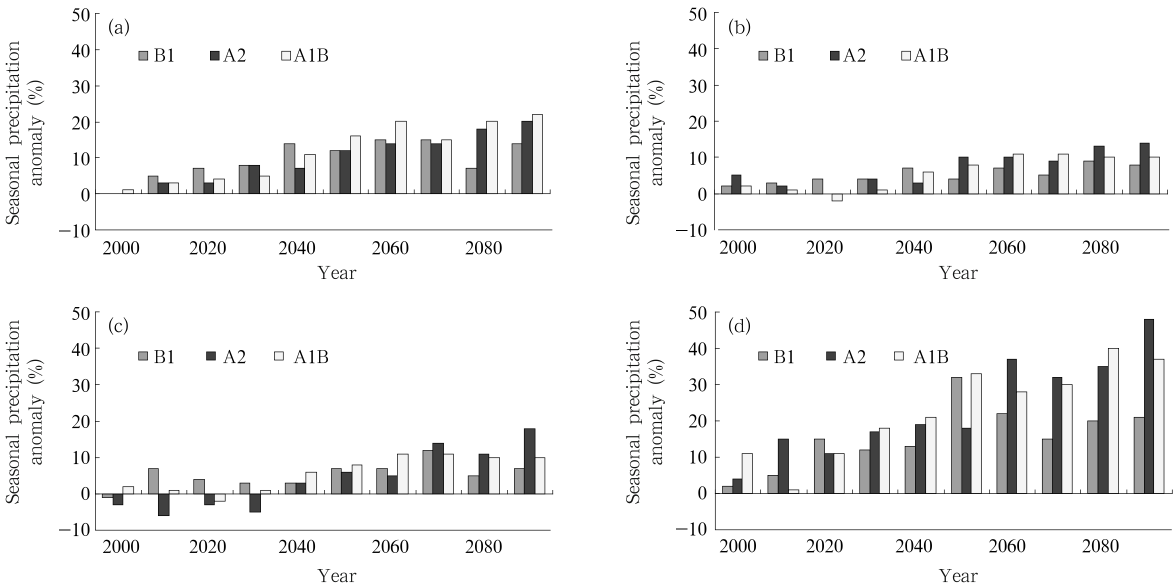

Fig. 5. Normalized seasonal precipitation anomalies (%) in the HRB in the 21st century for (a) spring, (b) summer, (c) autumn, and (d) winter.

not differ significantly from the 2020s to the 2040s, but the differences among them become increasingly obvious with time. The magnitude of the precipitation increase at the end of the 21st century is about two times higher under the highest emission scenario (A2) than under the lowest scenario (B1). The relative increases of winter precipitation in the 2090s under SRES scenarios A2 and B1 are approximately 48% and 21%, respectively. The relative increase of precipitation in spring is approximately 20% by the end of the 21st century, a little lower than the increase in winter. Precipitation in summer is expected to increase only slightly before the 2040s, and the differences between different emission scenarios are inconspicuous. Precipitation in autumn is projected to decrease slightly before the 2040s under SRES A2, then increase steadily, with a total increase of about 18% by the end of the 21st century.

Normalized monthly precipitation anomalies in the HRB are calculated for the 2020s and 2080s (Fig. 6). These indicate the changes during the early and later periods of the 21st century, respectively. The results suggest that the increase of precipitation is the largest in February and December, and smallest in November. The magnitude of the precipitation change under the lower greenhouse gas emission scenario (B1) is similar during the two periods; however, obvious fluctuations occur under the higher emission scenarios (A1B and A2). For example, precipitation is projected to decrease by about 4.5% in June, August, and September, but increase by 18.3% in February. Furthermore, in the 2080s, the projected maximum increase of precipitation reaches 50.7% in February but only 4.3% in November.

The spatial distribution of normalized annual precipitation anomalies in the 2020s and 2040s under the moderate emission scenario A1B is shown in Fig. 7. Precipitation is projected to increase mainly in eastern HRB in the 2020s, with smaller increases in other parts of the HRB (especially northern Shanxi Province). The precipitation increase is projected to become much more pronounced in the 2040s relative to the 2020s, with relative increases of approximately 8% in Beijing and Tianjin. The projected precipitation increase is most obvious in winter, with a maximum increase of approximately 20% centered around Shanxi and Hebei provinces under SRES A2 (figure omitted).

5.2 Changes in the water vapor budget

The results presented in Section 5.1 show that

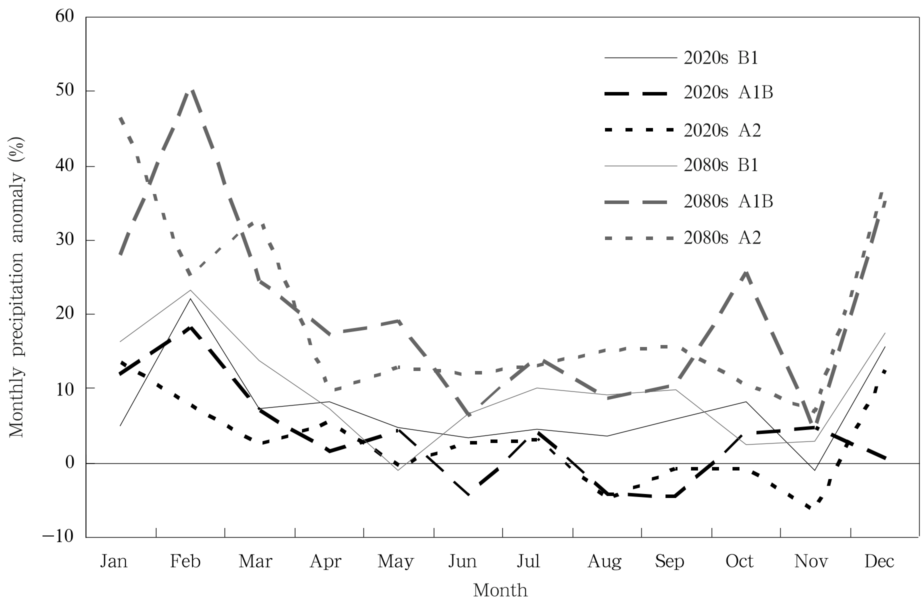

Fig. 6. Normalized monthly precipitation anomalies (%) in the HRB during the 2020s and 2080s.

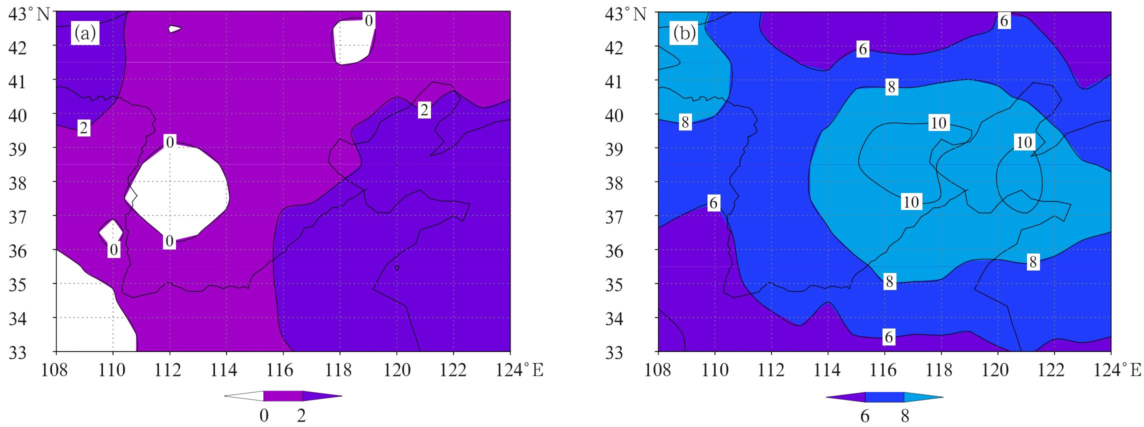

Fig. 7. Spatial distributions of normalized annual precipitation anomaly (%) in (a) the 2020s and (b) the 2040s under SRES A1B.

precipitation in the HRB is expected to increase in the 21st century. The linear trends of surface air temperature in the HRB from the IPCC AR4 multi-model ensemble mean indicate a persistent warming in the future, with annual mean surface air temperature increasing by 0.23, 0.39, and 0.42°C (10 yr)$^{-1}$ under SRES B1, A1B, and A2, respectively. The magnitude of the warming is projected to reach 2.4–4.6°C by the end of 2090s. As 70% of the total area of the earth is covered by ocean, global warming could result in increasing evaporation and an increase in the water vapor content of the atmosphere, especially over the ocean. Increasing temperature also enhances the capacity of the atmosphere to hold water vapor. According to the Clausius-Clapeyron equation (Clapeyron, 1834; Clausius, 1850), the saturation specific humidity increases by about 7% per degree Celsius increase in temperature. This enhanced holding capacity results in both specific humidity and saturation specific humidity increasing as the atmosphere warms, with relative humidity remaining nearly constant. Under more significant temperature increases with smaller specific humidity increases, relative humidity would decrease, reducing the possibility of precipitation and increasing the likelihood of drought occurrences. By contrast, if specific humidity were to increase by a large enough amount such that the relative humidity increases, precipitation and precipitation intensity would also increase. The specific humidity only quantifies the amount of water vapor in the atmospheric column; constant convergence of water vapor is necessary for precipitation formation. However, the station-observed evaporation in many regions from evaporating dish experienced decreases with the increasing temperature in recent 50 years. This is contrary to the Clausius-Clapeyron equation. The reason is complex and may involve global dimming, wind speed changes, and so on.

Changes in the water vapor budget and atmospheric moisture over the HRB are discussed in this section. The results in this section are from the five-model ensemble mean mentioned in Section 4 under SRES A1B. One reason is that some individual models did not submit the necessary variables for calculations of water vapor fluxes and relative humidity to IPCC AR4 data archive; another is consideration of the models' relative capabilities in the HRB region. Figure 8 shows the evolution of regional anomalies of surface air temperature, precipitation, and probable precipitation relative to the average of 1980–1999. Probable precipitation is projected to increase steadily, with a trend similar to that of temperature. Precipitation increases abruptly after the 2040s, consistent with the results from ensemble mean of all IPCC AR4 models discussed in Section 5.1.

Figure 9 shows the spatial distributions of summer total column water vapor content anomalies in the 2040s and 2080s. These anomalies suggest that probable precipitation will increase in the future, especially toward the end of the 21st century. The increase of water vapor content is more pronounced at mid-lower latitudes than at higher latitudes. This feature has also been discussed by Sun and Ding (2008). Some previous studies suggest that water vapor transport will increase in eastern China in the future (Li et al., 2008) owing to the stronger southerly wind in the monsoon region east of 105°E. Some recent studies also indicate that the East Asian summer monsoon will be intensified in the 21st century (Sun and Ding, 2008; Li et al., 2008). The stronger southwesterly wind is expected to bring more warm and vapor-rich air to northern regions. We also calculate the water vapor

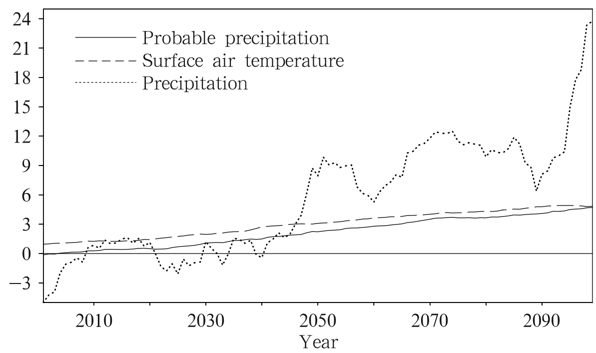

Fig. 8. Linear trends of anomalies in probable precipitation (black solid curve; kg m^{-2}), surface air temperature (long dashed curve; ℃), and precipitation (short dashed curve; %) under SRES A1B in the 21st century.

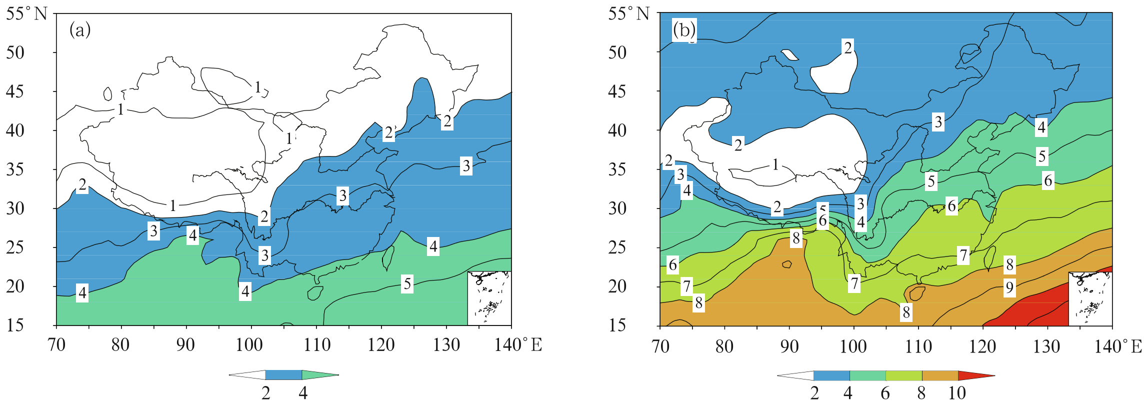

Fig. 9. Total column water vapor content anomalies (kg m^{-2}) in summer for (a) the 2040s and (b) the 2080s.

transport across the four boundaries of the HRB, along with the net budget. The results indicate that the transport of water vapor across the southern boundary increases significantly compared to that during 1980–1999; however, the net water vapor budget in the region changes little because the water vapor output through the eastern border is also projected to increase in the future.

Relative humidity (RH) anomalies in the HRB relative to the 1980–1999 mean (within the region of 35°–43°N, 112°–120°E) have been calculated. The trends vary with height (Fig. 10a). The time-height cross-section of RH anomalies indicates a decrease in atmospheric RH below 400 hPa, especially in the lowermost atmosphere, below 850 hPa. RH increases substantially in the stratosphere after 2040. These results are consistent with those reported by Lorenz and Deweaver (2007). They showed that RH tends to decrease in the subtropics and midlatitudes at lower levels, but increases poleward of 50° (their Fig. 2). The time-height cross-section of specific humidity anomalies (σq) (Fig. 10b) shows trends that contrast with the RH trends, with increases in the troposphere but only small changes at levels above 300 hPa. The saturation specific humidity anomalies ($\sigma q_{\rm s}$) also experience increasing trends below 300 hPa (Fig. 10c); however, the magnitude of $\sigma q_{\rm s}$ is larger than that of q, thus resulting in the decreasing trend in RH (see Eq. (11)). Although the volume of water vapor in the atmosphere increases with global warming, this increase does not imply an inevitable increase in precipitation. Constant convergence and transport of water vapor are also required for the occurrence of precipitation. Increases in the water vapor content of the

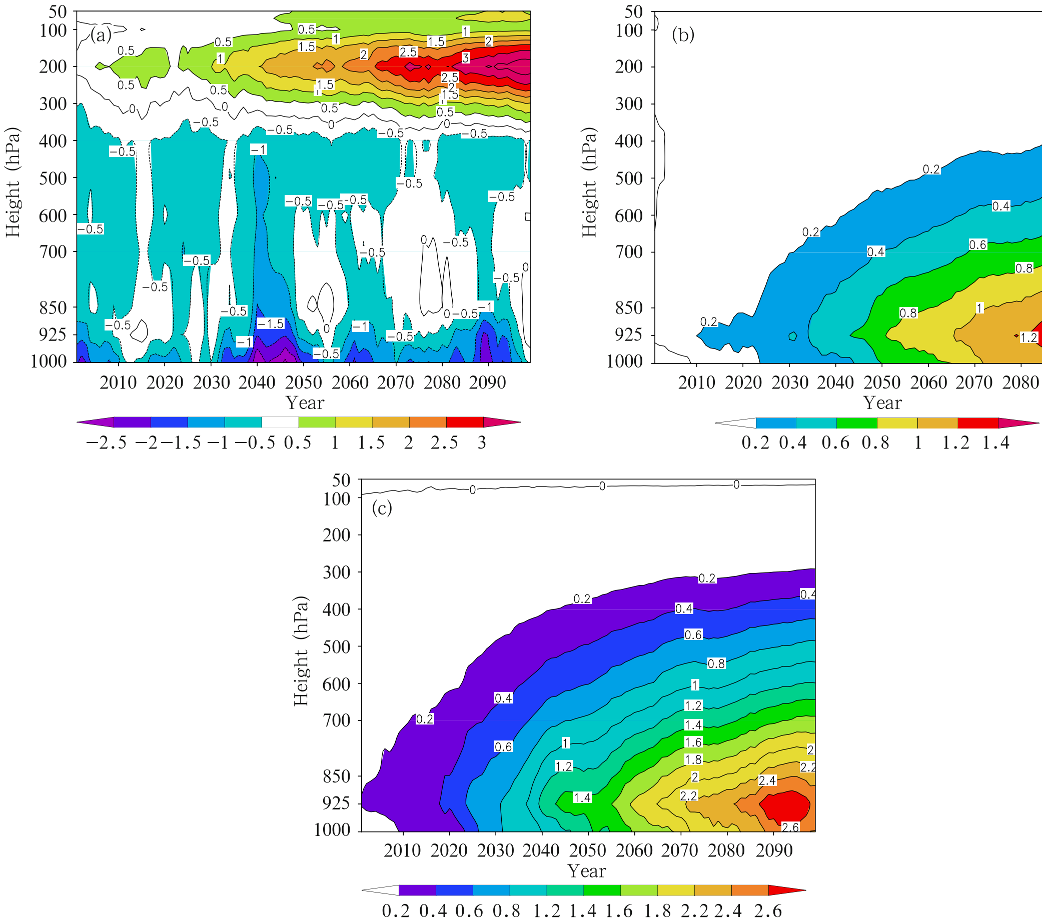

Fig. 10. Time-height cross-section of anomalies of (a) relative humidity (%), (b) specific humidity (g kg^{-1}), and (c) saturation specific humidity (g kg^{-1}) over the HRB.

atmosphere with increasing temperature still might lead to regional droughts or floods due to the effects of these dynamical factors.

5.3 Changes in the atmospheric water cycle

The drying and poleward expansion of the subtropics and the moistening of the deep tropics and mid to high latitudes are robust model projections of climate change forced by rising greenhouse gases. These changes are often summarized as "rich-getting-richer" or "dry-getting-drier and wet-getting-wetter". That is, the already wet areas in the deep tropics and midlatitudes are projected to get wetter, while the arid and semiarid regions of the subtropics are projected to get drier (Seager et al., 2010; Held and Soden, 2006; Chou et al., 2009). Such large-scale changes to the hydrological cycle, if they occur, will have important consequences for human societies and ecosystems.

We calculate the changes of precipitation P minus evaporation E (P–E) for the five-model ensemble mean. Monthly surface latent heat flux is taken from the IPCC AR4 online archive (refer to Section 2.1 for the website address). To convert evaporation from energetic to mass-based units, we divide the surface latent heat flux by the latent heat of vapourisation.

Figure 11a shows the annual mean of P–E for the baseline period 1980–1999. The models produce negative P–E over the HRB, which means that E exceeds P in this region. P–E is most strongly negative along the eastern coastline. Persistent drought occurred during this period (Section 3). Both precipitation and evaporation are projected to increase in the 21st century (relative to 1980–1999). Figure 11b shows the annual mean differences of evaporation in the 2040s relative to the baseline period under SRES A1B. The trend in evaporation is consistent with the trend in precipitation (Fig. 7b). In the 2040s, the annual mean P–E is enhanced in land but reduced over the ocean (Fig. 11c). These same spatial patterns are found throughout the whole 21st century. The annual

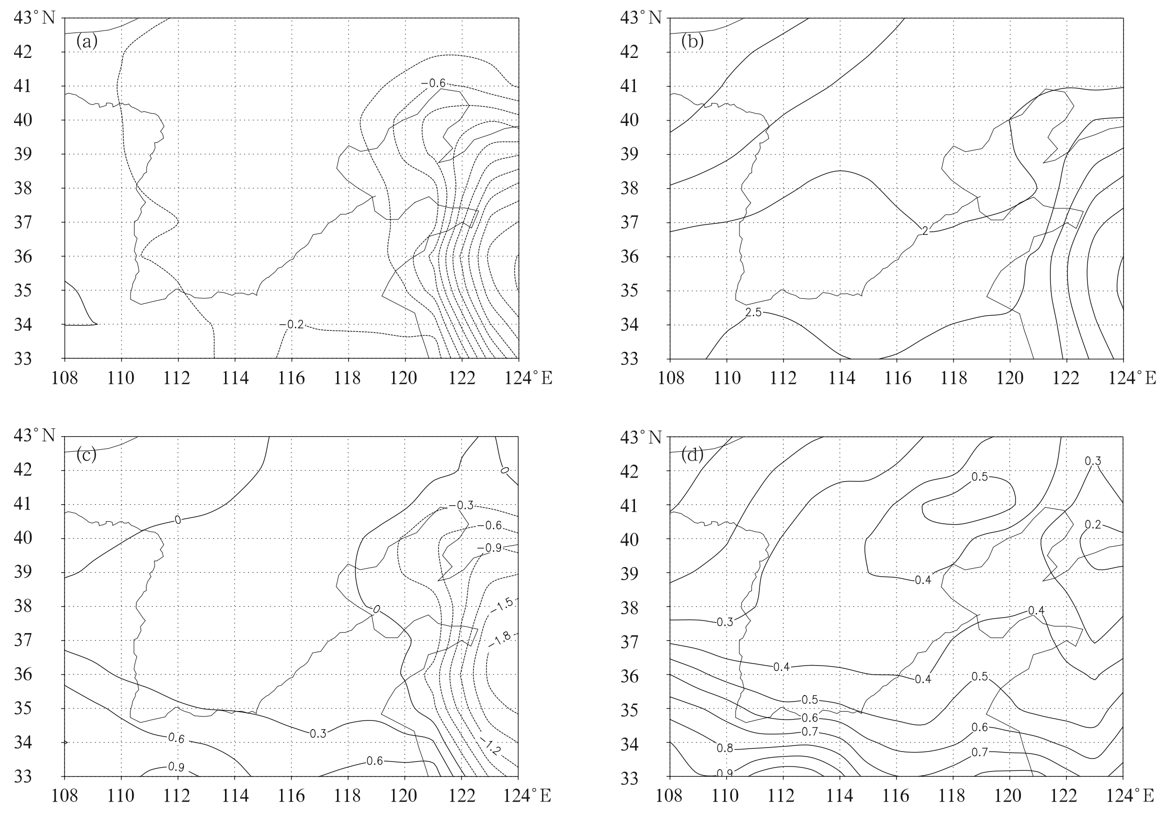

Fig. 11. (a) Annual mean of P–E in 1980–1999, (b) annual change of E in the 2040s under SRES A1B, (c) annual mean of P–E in the 2040s, and (d) annual change of P–E in the 2040s. Unit: mm day^{-1}.

mean P–E during the 2040s is substantially increased relative to 1980–1999, by about 0.4 mm day^{-1} in most regions (Fig. 11d). The changes in P, E, and P–E in summer are similar to the changes in the annual means. The projections therefore indicate that the HRB is expected to get wetter in the 21st century due to global warming.

The above analysis illustrates that the general rules of "poor-getting-poorer" and "rich-getting-richer" are not always satisfied on the regional scale. Held and Soden (2006) pointed out that a warming atmosphere will cause an increase in atmospheric water vapor. Hence, even if the circulation were to remain fixed, it would be expected that the transport of water vapor would intensify. Under these assumptions, the pattern of P–E would remain the same but the values would become more extreme, making wet regions wetter and dry regions drier. They considered only the thermodynamic contributions to the changes in P–E in their calculations. However, changes in the mean circulation also contribute significantly to changes in P–E particularly on the poleward margins of the subtropical dry zones (Seager et al., 2010). While these subtropical changes are known to be related to the projected expansion of the Hadley cell (Lu et al., 2007) and poleward shift of the storm tracks (Yin, 2005), the exact dynamical mechanisms underlying these changes remain unclear (Chen et al., 2008). In addition, there are some other factors that are also partly responsible. Much work remains to be done in unraveling the relative importance of these and other processes in determining the ways that global warming affects the hydrological cycle.

P–E is the most important factor in the net flux of water substance at the earth's surface; however, a number of other factors also play important roles, such as plant transpiration, water vapor transport, surface runoff, infiltration, and so on. Projections of future changes in the water cycle are far more complex than projections of future temperature changes, even without considering important local seasonal differences in the responses of the water cycle to climate change.

6. Conclusions and discussion

The climatological characteristics of precipitation and the water vapor budget in the HRB over the most recent 50 years have been analyzed using observation data from 740 stations in China and the ERA40 reanalysis data. Further, projected future changes in precipitation and the water vapor budget have been discussed in the context of the IPCC AR4 multi-model ensemble results under SRES scenarios B1, A1B, and A2. The main conclusions are as follows.

(1) Precipitation and surface air temperature in the HRB have experienced significant interdecadal variations. Conditions were relatively cold and wet before the 1970s but relatively warm and dry after the 1980s. Precipitation has decreased substantially, especially since the 1990s, and surface air temperature continues to rise. The total column water vapor has also decreased remarkably since the late 1970s due to a decrease in the influx of water vapor through the southern border of the HRB region.

(2) The IPCC AR4 multi-model ensemble is capable of simulating many of the 20th century climate features, and can successfully reproduce the spatial patterns of precipitation and temperature. Unfortunately, the multi-model ensemble does not reproduce the interdecadal change during the 1980s.

(3) Relative to the models' baseline climatology averaged from 1980–1999, precipitation is expected to increase in the 21st century under all three SRES scenarios, with obvious interannual fluctuations before the 2040s. The increase in precipitation is expected to be more pronounced following the 2040s, with precipitation increasing by 10%–18% by the end of the 21st century.

(4) Due to the persistent warming of surface air temperature, water vapor content in the lower atmosphere is projected to increase substantially. Relative humidity is projected to decrease in the mid-lower troposphere but increase in the upper troposphere. The regional net water vapor budget in the HRB does not change appreciably, since both water vapor input through the southern border and water vapor output through the eastern border increase simultaneously. On the other hand, precipitation minus evaporation increases during the 21st century. Based on these results, the HRB is expected to get wetter in the 21st century due to global warming.

This study indicates that both precipitation and water vapor in the atmosphere over the HRB are likely to increase in the 21st century; however, the increase in surface air temperature is more pronounced. Climate change can influence the water cycle in many ways: one is by increasing the actual water vapor content in the atmosphere through enhanced evaporation from the ocean surface and by increasing the capacity of the atmosphere to hold water vapor due to increases in temperature; another is by modifying water vapor transport by changing the regional atmospheric circulation. When the meridional circulation patterns prevail, zonal transport of water vapor is blocked. The development of abnormal moisture convergence and divergence areas results in the development of rainstorm areas and coexisting arid areas. It is therefore very challenging to predict whether the climatology of the HRB changes from warm-dry to warm-wet or not. It is also difficult to accurately determine the future trends and characteristics of the spatial-temporal distribution of water resources using only projections of precipitation and water vapor from climate models. Further research on the response of regional water resources to climate change will require the application of hydrological models.

It is well known that the current generation climate models is more uncertain about the global-mean precipitation response to global warming than the temperature response (Meehl et al., 2005). The models adopted by the IPCC AR4 are substantially improved relative to those presented in the IPCC TAR (IPCC, 2001). However, we have identified several obvious differences between various scenarios and individual model results in the current analysis, especially in the mid-later periods of the 21st century. These uncertainties result mainly from the feedback processes and capabilities of the models, as well as differences in greenhouse gas emission scenarios and other factors. The carbon cycle has been coupled into most climate models contributing to the Fifth Assessment Report of the IPCC (IPCC AR5)(http://www.ipcc.ch), and the emission scenarios and experimental conditions adopted by the IPCC AR5 are also better constrained. The output from these models will be released in 2012. This may facilitate the ability to obtain more credible results and to undertake detailed comparisons with results of this study. The analysis of HRB regional climate change will also require the application of downscaling methods to capture regional features in greater detail.

Acknowledgments. We acknowledge the IPCC AR4 modeling groups for providing their data for the present analysis. The Program for Climate Model Diagnosis and Intercomparison (PCMDI) and the World Climate Research Programme (WCRP) Coupled Model Intercomparison Project are thanked for their collecting and archiving the model output and organizing the model data analysis activity. The ensemble data have been collected, analyzed, and processed by the National Climate Center of China.

REFERENCES

Chen, G., J. Lu, and D. Frierson, 2008: Phase speed spectra and the latitude of surface westerlies: Interannual variability and global warming trend. *J. Climate*, **21**, 5942–5959.

Chou, C., J. D. Neelin, C. A. Chen, et al., 2009: Evaluating the “rich-get-richer” mechanism in tropical precipitation change under global warming. *J. Climate*, **22**, 1982–2005.

Clausius, R., 1850: Ueber die bewegende Kraft der Wärme und die Gesetze, welche sich daraus für die Wärmelehre selbst ableiten lassen. *Annalen der Physik*, **155**, 500–524.

Clapeyron, M. C., 1834: Mémoire sur la puissance motrice de la chaleur. *Journal de l'École Polytechnique*, **23**, 153–190.

Ding Yihui, 1989: *Diagnostic and Analytical Methods in Synoptic Dynamics*. Science Press, Beijing, 44–45. (in Chinese)

Grossmann, A., and J. Morlet, 1984: Decomposition of Hardy functions into square integrable wavelets of constant shape. *Slam J. Math. An.*, **15**, 723–736.

Guo Hua, Su Buda, Wang Yanjun, et al., 2007: Runoff coefficients change and the analysis of the relationship between climate factors and runoff coefficients in Poyang Lake basin: 1955–2002. *J. Lake Sci.*, **19**(2), 163–169. (in Chinese)

Held, I. M., and B. J. Soden, 2006: Robust responses of the hydrological cycle to global warming. *J. Climate*, **19**, 5686–5699.

IPCC, 2001: *Climate Change 2001: The Scientific Basis.*

Cambridge University Press, Cambridge, UK, 881 pp.

IPCC, 2007: *Climate Change, 2007: The Physical Science Basis*. Cambridge University Press, Cambridge, United Kingdom and New York, NY, USA, 996 pp.

Jiang Dabang, Wang Huijun, and Lang Xianmei, 2005: Evaluation of East Asian climatology as simulated by seven coupled models. *Adv. Atmos. Sci.*, **22**, 479–495.

—-, Zhang Ying, and Sun Jianqi, 2009: Ensemble projection of 1–3℃ warming in China. *Chinese Sci. Bull.*, **54**(24), 3870–3877. (in Chinese)

Jiang Tong, Su Buda, Wang Yanjun, et al., 2005: Trends of temperature, precipitation and runoff in the Yangtze River basin from 1961 to 2000. *Adv. Climate Change Res.*, **1**(2), 65–68. (in Chinese)

Kendall, M. G., 1975: *Rank Correlation Methods. 4th Edition*. Griffin, London, 160 pp.

Li Qiaoping, Ding Yihui, and Dong Wenjie, 2008: Summer precipitation change over eastern China in future 30 years under SRES A2 scenario. *J. Appl. Meteor. Sci.*, **19**(6), 770–780. (in Chinese)

Liu Luliu, Liu Zhaofei, and Xu Zongxue, 2008: Trends of climate change for the upper-middle reaches of the Yellow River in the 21st century. *Adv. Climate Change Res.*, **4**(3), 167–172. (in Chinese)

Liu Min and Jiang Zhihong, 2009: Simulation ability evaluation of surface temperature and precipitation by thirteen IPCC AR4 coupled climate models in China during 1961–2000. *J. Nanjing Institute of Meteor.*, **32**(2), 256–268. (in Chinese)

Lorenz, D. J., and E. T. DeWeaver, 2007: The response of the extratropical hydrological cycle to global warming. *J. Climate*, **20**, 3470–3484.

Lu, J., G. Vecchi, and T. Reichler, 2007: Expansion of the Hadley cell under global warming. *Geophys. Res. Lett.*, **34**, L06805, doi: 10.1029/2006GL028443.

Mann, H. B., 1945: Nonparametric tests against trend. *Econometrica*, **13**, 245–259.

Meehl, G. A., C. Covey, B. McAvaney, et al., 2005: Overview of the coupled model intercomparison project. *Bull. Amer. Meteor. Soc.*, **86**, 89–93.

Seager, R., N. Naik, and G. A. Vecchi, 2010: Thermodynamic and dynamic mechanisms for large-scale changes in the hydrological cycle in response to global warming. *J. Climate*, **23**, 4651–4668.

Shi Yafeng, Liu Chunzhen, and Zhang Xiangsong, 1995: *Influence of Climatic Change to Water Resources on the Northwest and North China*. Shandong Technology Press, Jinan, 369 pp. (in Chinese)

Sun Ying and Ding Yihui, 2008: An assessment on the performance of IPCC AR4 climate models in simulating interdecadal variations of the East Asian summer monsoon. *Acta Meteor. Sinica*, **66**(5), 765–780. (in Chinese)

Wang Jinxia and Huang Jikun, 2004: Water issues in the Fuyang River basin. *J. Natural Resources*, **19**(4), 424–429. (in Chinese)

—-, Li Hao, Xia Jun, et al., 2008: Water shortage and adaptation measures under climate change: Simulation analysis in the Haihe River basin. *Adv. Climate Change Res.*, **4**(6), 336–341. (in Chinese)

Water Resources Committee for the Haihe River Basin, 2006: *Water Resource Bulletin in Haihe River*. Tianjin, 25 pp. (in Chinese)

Wei Fengying, 2007: *Statistics Technology of Diagnose and Forecast of Modern Climate*. China Meteorological Press, Beijing, 57–70. (in Chinese)

Xu Conghai, Shen Xinyong, and Xu Ying, 2007: An analysis of climate change in East Asia by using the IPCC AR4 simulations. *Adv. Climate Change Res.*, **3**, 287–291. (in Chinese)

Ye Duzheng and Huang Ronghui, 1996: *Study on Drought and Flood Laws and Causes in the Yangtze River and the Yellow River*. Shandong Technology Press, Jinan, 387 pp. (in Chinese)

Yin, J. H., 2005: A consistent poleward shift of the storm tracks in simulations of 21st century climate. *Geophys. Res. Lett.*, **32**, L18701, doi: 10.1029/2005GL023684.

Zhang Li, Ding Yihui, and Sun Ying, 2008: Evaluation of precipitation simulation in East Asian monsoon areas by coupled ocean-atmosphere general circulation models. *Chinese J. Atmos. Sci.*, **32**(2), 261–276. (in Chinese)

Zhang Liping, Xia Jun, Lin Zhaohui, et al., 2008: Variation and transport feature of atmospheric water resources in Haihe River basin. *J. Hyd. Eng.*, **39**(2), 206–217. (in Chinese)

Zeng Xiaofan, Su Buda, Jiang Tong, et al., 2007: Projection of future climate change in the Yangtze River basin for 2001–2050. *Adv. Climate Change Res.*, **3**(5), 293–298. (in Chinese)

Zhou Tianjun and Yu Rucong, 2006: Twentieth-century surface air temperature over China and the global simulated by coupled climate models. *J. Climate*, **19**, 5843–5858.